INTERNATIONAL JOURNAL FOR NUMERICAL METHODS IN FLUIDS
*Int. J. Numer. Meth. Fluids* 2002; **39**:23–40 (DOI: 10.1002/fld.260)

# Numerical simulation of laminar flow and heat transfer over banks of staggered cylinders

D. Ghosh Roychowdhury[1], Sarit Kumar Das[2] and T. Sundararajan[2,*,†]

[1] *Core Engineering Section, Design & Technology Group, Indira Gandhi Centre for Atomic Research, Kalpakkam—603 102, India*
[2] *Mechanical Engineering Department, Indian Institute of Technology Madras, Chennai—600 036, India*

## SUMMARY

A study is conducted to investigate forced convective flow and heat transfer over a bank of staggered cylinders. Using a novel numerical formulation based on a non-orthogonal collocated grid in a physical plane, the effects of Reynolds number and cylinder spacing on the flow and heat transfer behaviour are systematically studied. It is observed that both the Reynolds number and cylinder spacing influence the recirculatory vortex formation and growth in the region between the cylinders; in turn, the rates of heat transfer between the fluid and the staggered cylinders are affected. As the cylinder spacing decreases, the size and length of eddies reduce. For sufficiently small spacings, eddy formation is completely suppressed even at high Reynolds number. Pressure drop and Nusselt number predictions based on numerical study are in excellent agreement with available correlations. The study provides useful insight on the detailed flow and heat transfer phenomena for the case of a bank of staggered cylinders. Copyright © 2002 John Wiley & Sons, Ltd.

KEY WORDS: N–S equation; non-orthogonal; collocated; laminar flow; forced convection; cylinders; staggered

## INTRODUCTION

The studies on pressure drop and heat transfer characteristics for cross flow over tube banks continue to attract considerable interest amongst researchers because of the importance of this configuration to heat exchangers. Most of the early works on this topic are experimental in nature and they provide correlations for pressure drop and heat transfer coefficients for both in-line and staggered banks of tubes. Pierson [1] and Bergelin *et al.* [2, 3] are among the early ones who investigate the flow phenomena around in-line and staggered tube banks. Zhukauskas' [4] excellent survey of the experimental studies on flow over tube banks provides valuable insight on the associated transport phenomena. Subsequently, the correlations suggested by him are used for designing full-scale heat exchanger apparatus.

*Correspondence to: T. Sundararajan, TDCE Laboratory, Mechanical Engineering Department, Indian Institute of Technology Madras, Chennai—600 036, India.
†E-mail: tsundar@acer.iitm.ernet.in

*Received October 2000*
*Revised September 2001*

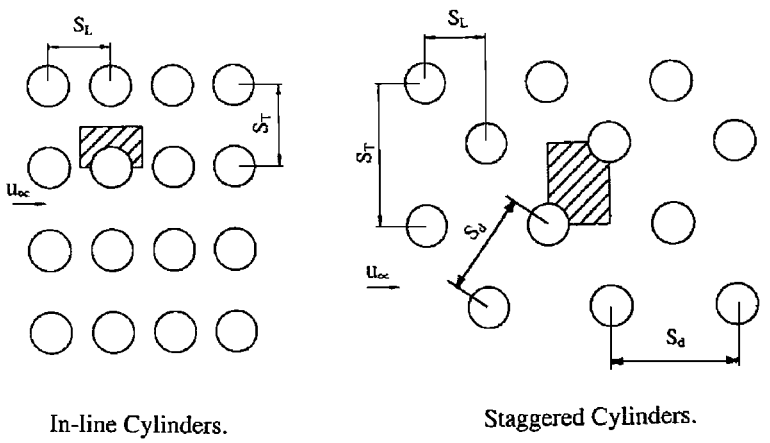


Figure 1. Computational domain for flow over a bank of cylinders.

While experimental studies provide useful correlations between the global parameters for such complex problems, obtaining detailed information about the flow and temperature fields experimentally is expensive and cumbersome. Numerical simulation studies are economical alternatives for gaining a deep understanding of the associated flow and thermal phenomena, and their effects upon the heat transfer rate and pressure drop. Simulation of flow and heat transfer for the entire tube bank geometry requires extensive computational resources. A useful approximation, in this regard, is the 'periodically developed flow' assumption. According to this assumption, the interaction between two neighbouring cylinders in the interior region of the tube bank can be represented by a globally developed (but locally varying flow field) with a fixed pressure drop and temperature increment per row of tubes. Hence, the main features of the flow and heat transport processes could be understood by simulating one typical cell (covering the region between two adjacent tubes), as shown in Figure 1 (a) and (b).

Earlier numerical studies on the simulation of flow and heat transfer over tube banks have employed co-ordinate transformation using body-fitted grids [5], or step-like Cartesian grids [6, 7] or chimera type embedded grids [8]. Some extra effort for the grid generation process and additional book-keeping are the difficulties associated with such approaches. Recently, the present authors have developed a novel non-orthogonal, collocated grid based solution procedure [9] for simulating laminar viscous flows. The method solves for the flow field in the physical plane itself directly, without any co-ordinate transformation. Therefore, the coefficients of the flow variables in the discretized equation can be directly linked to the corresponding areas or lengths, thereby retaining physical insight in the finite volume procedure. On the other hand, the choice of curvilinear contravariant or covariant velocity components as cell face velocities involve complicated tensor algebra to derive the momentum equations in the transformed domain. Also, additional curvature terms are present in the governing equations, which need to be treated as source terms. In view of these, it is difficult to control or check physical flux balances during computation in the transformed domain. As a consequence, the rate of convergence is severely affected, especially for highly skewed meshes. In the present

 

study, the novel algorithm is implemented for the complex situation of flow over a bank of staggered cylinders. Periodic boundary conditions are implemented at inlet and exit planes of the computational region [10, 11], assuming periodically developed flow. The predicted flow and heat transfer results are validated with the results of Bergelin *et al*. [3] and Zhukauskas and Ulinkas [12] for in-line tube bank array and with Zhukauskas and Ulinkas [12] and Chen and Wung [13] for staggered tube bank array. Also, a detailed parametric study involving steady state laminar flow and heat transfer over a bank of staggered cylinders is presented for different spacings and flow Reynolds numbers. The predicted pressure drop and Nusselt number variations are explained in terms of the changes in flow structure, for the range of conditions studied.

## GOVERNING EQUATIONS AND DISCRETIZATION

Under the assumption of incompressible flow, without viscous dissipation and absence of body forces, the governing equations for mass conservation and transport of momentum and energy can be expressed in integral form, using the Cartesian tensor notation, as follows.

Continuity:

$$\int_A \rho u_j n_j \, \mathrm{d}A = 0 \tag{1}$$

Momentum:

$$\frac{\partial}{\partial t}\int_V (\rho u_i)\, \mathrm{d}V + \int_A (\rho u_i u_j) n_j \, \mathrm{d}A = -\int_A P n_i \, \mathrm{d}A + \int_A \tau_{ij} n_j \, \mathrm{d}A \tag{2}$$

where $\tau_{ij} = \mu\left[\dfrac{\partial u_i}{\partial x_j} + \dfrac{\partial u_j}{\partial x_i}\right]$ and $P$ is the dynamic pressure.

Energy:

$$\frac{\partial}{\partial t}\int_V (\rho C_P T)\, \mathrm{d}V + \int_A (\rho C_P T u_j) n_j \, \mathrm{d}A = \int_A \left(\lambda \frac{\partial T}{\partial x_j}\right) n_j \, \mathrm{d}A + \int \dot{Q}\, \mathrm{d}V \tag{3}$$

Since the details of the non-orthogonal grid based viscous flow in the two-dimension algorithm are described elsewhere [9], only the basic steps are recounted here for the sake of completeness. The extension of the same algorithm in three dimensions is straightforward.

Integration of the above governing equations over a control volume (Figure 2(a)) yields the following form of discretized equations:

Continuity:

$$F_e - F_w + F_n - F_s = 0 \tag{4}$$

where $F_k = \sum \rho_k \Phi_k A_{kj}; \Phi \Rightarrow u, v; k \rightarrow e, w, n, s;$ and $j \Rightarrow x, y$

In the above expressions, $A_{kj}$ represents the projected area in $x$ or $y$ direction for the $k$th side of the control volume (Figure 2(b)).

Momentum and Energy:

$$a_P^* \Phi_P = a_E \Phi_E + a_W \Phi_W + a_N \Phi_N + a_S \Phi_S + S_P + \frac{\rho V_P}{\Delta t}\Phi_P^o \tag{5}$$

 

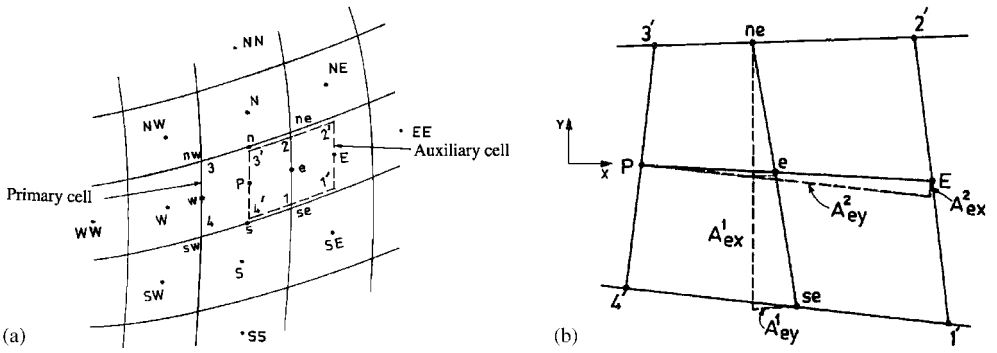


Figure 2. (a) Typical control volume; (b) area vectors for face $e$.

where

$$a_E = \| - F_e, 0\| + d_e^1, \quad a_W = \|F_w, 0\| + d_w^1$$

$$a_N = \| - F_n, 0\| + d_n^1, \quad a_S = \|F_S, 0\| + d_s^1$$

$$a_P^* = a_E + a_W + a_N + a_S + \frac{\rho V_P}{\Delta t}, \quad S_P = b_{no} + b_{QU} + S_\Phi$$

$b_{QU}$ is the source term arising from the deferred correction by QUICK scheme; $b_{no}$ is a source term arising due to non-orthogonal grid contributions $= (d_e^2 + d_n^2)\Phi_{ne} - (d_w^2 + d_n^2)\Phi_{nw} - (d_e^2 + d_s^2)\Phi_{se} + (d_w^2 + d_s^2)\Phi_{sw}$.

$S_\phi$ is a source term; $= \delta P_i$ for momentum equation and, $= \dot{Q}_P V_P / C_P$ for energy equation in the case of heat generation.

In the above expressions, $d_e^1 = \Gamma_e / V_e [A_{ex}^1 A_{ex}^1 + A_{ey}^1 A_{ey}^1]$ is the orthogonal part of diffusive flux on east face, and $d_e^2 = \Gamma_e / V_e [A_{ex}^1 A_{ex}^2 + A_{ey}^1 A_{ey}^2]$ is the non-orthogonal part of diffusive flux on east face, where $\Gamma \Rightarrow \mu$ for momentum equation and $(\lambda / C_P)$ for energy equation.

Similar expressions can be obtained for the other faces, $w, n$ and $s$. The pressure term is defined as

$$\delta P_i = \delta P_x = A_{Px}^1 (P_w - P_e) + A_{Px}^2 (P_s - P_n) = \text{in } x \text{ momentum equation} \quad \text{and}$$

$$\delta P_i = \delta P_y = A_{Py}^1 (P_w - P_e) + A_{Py}^2 (P_s - P_n) = \text{in } y \text{ momentum equation}$$

Normally, the Equation (5) can be expressed in under-relaxed form as

$$a_P \Phi_P = \sum a_{nb} \Phi_{nb} + S_P + (1 - \alpha_\phi)\Phi_P^0 + \frac{\rho V_P}{\Delta t} \Phi_P^0 \tag{6}$$

where $\Phi$ represents $u, v$ and $T$; and $\alpha_\phi =$ under-relaxation factor for the variable $\Phi$.

The continuity Equation (1) is satisfied with the help of a pressure-correction equation [14] of the form

$$a_P P_P' = \sum a_{nb} P_{nb}' + b_P + b_{Pno} \tag{7}$$

 

which is derived by evaluating the cell face velocities from Equation (6) using the Pressure Weighted Interpolation Method-Corrected (PWIMC) of Kobayashi and Pereira [15].

In the above equation, $b_{Pno}$ represents the source term for the pressure correction equation arising due to non-orthogonality of the grid and $b_P$ is the source term, which is the residue of continuity equation, i.e.

$$b_P = -[F_e^* - F_w^* + F_n^* - F_s^*] \tag{8}$$

In the present algorithm, the contributions due to non-orthogonal terms are neglected altogether in the pressure correction equation, in order to achieve a faster rate of convergence. Hence, the final form of pressure correction equation becomes

$$a_P P'_P = \sum a_{nb} P'_{nb} + b_P \tag{9}$$

The pressure corrections $P'$ thus obtained are multiplied by an under-relaxation factor $\alpha_P$ and then added with the guess pressure values ($P^*$) to evaluate the final pressure values ($P$) through the expression

$$P = P^* + \alpha_P P' \tag{10}$$

For all the numerical simulations, the following convergence criteria were used:

(i) the maximum residual at any point normalized by $\rho Au^2$ for momentum equations, $\rho Au$ for pressure equation and $\rho C_P AuT$ for energy equation $\leqslant 10^{-5}$;
(ii) maximum normalized difference in individual components ($u, v, P$ and $T$) with respect to previously iterated value $\leqslant 10^{-5}$.

The QUICK scheme as a deferred correction to first order upwind scheme is used for discretizing the convective fluxes. Initial relaxation factors are taken as $\alpha_u = 0.3$, $\alpha_P = 0.1$ and $\alpha_t = 0.3$ and these are progressively increased to $\alpha_u = 0.5$, $\alpha_P = 0.3$ and $\alpha_t = 0.5$ to accelerate convergence.

*Boundary conditions*

The flow through a regular array of cylinders is similar to flow through a straight pipe in the sense that there will be an entrance region beyond which the flow gets fully developed. In a passage of periodically varying cross-section, the fully developed flow is characterized by a velocity field that repeats itself at corresponding axial locations in successive cycles and the pressures at cyclically corresponding locations decrease linearly in the downstream direction. For steady flow over a bank of cylinders having a large number of rows, the flow can be assumed to be fully developed in the inner rows. Hence, the problem here is treated as a periodic flow with a constant pressure drop $\Delta P$ in the fully developed region. Since the cylinders are symmetrically placed, the computational domain is selected as shown in Figure 1.

(i) For in-line cylinders (Figure 3), the sides af and de are periodic boundaries on which symmetric periodic boundary conditions are specified, whereas ab, cd and ef are symmetric boundaries. The boundary conditions used are as follows:
- at inlet (af):

$$u(0, y) = u(l, y); \quad v(0, y) = v(l, y)$$
$$P(0, y) = P(l, y) + \Delta P$$

 

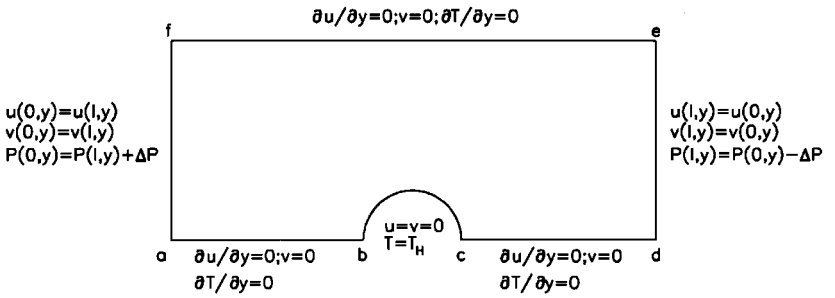


Figure 3. Boundary conditions for a bank of in-line cylinders.

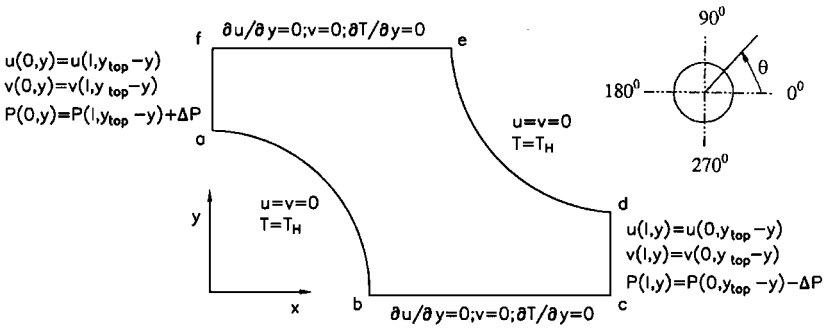


Figure 4. Boundary conditions for a bank of staggered cylinders.

- at outlet (de):

$$u(l, y) = u(0, y); \quad v(l, y) = v(0, y)$$
$$P(l, y) = P(0, y) - \Delta P$$

- at plane of symmetry (ab, cd and ef):

$$\partial u_\tau / \partial n = 0; \quad u_n = 0 \text{ and } \partial T / \partial n = 0$$
$$\text{i.e.} \quad \partial u / \partial y = 0; \quad v = 0 \text{ and } \partial T / \partial y = 0$$

- at the tube wall:

No slip condition and constant temperature are specified i.e. $u = v = 0$ and $T = T_H$.

(ii) For staggered cylinders (Figure 4), sides af and cd are periodic boundaries in which anti-symmetric periodic boundary conditions are specified, whereas bc and ef are symmetric boundaries. The boundary conditions are as follows:

 

- at inlet (af):

$$u(0, y) = u(l, y_{\text{top}} - y); \quad v(0, y) = v(l, y_{\text{top}} - y)$$
$$P(0, y) = P(l, y_{\text{top}} - y) + \Delta P$$

- at outlet (de):

$$u(l, y) = u(0, y_{\text{top}} - y); \quad v(l, y) = v(0, y_{\text{top}} - y)$$
$$P(l, y) = P(0, y_{\text{top}} - y) - \Delta P$$

- at plane of symmetry (bc and ef):

$$\partial u_\tau / \partial n = 0; \quad u_n = 0 \text{ and } \partial T / \partial n = 0$$
$$\text{i.e.} \quad \partial u / \partial y = 0; \quad v = 0 \text{ and } \partial T / \partial y = 0$$

- at the tube wall:
  No slip condition and constant temperature are specified i.e $u = v = 0$ and $T = T_H$.

For both in-line and staggered cases, in order to have a flow, it is necessary that the pressures at the inlet and outlet differ by a constant value $\Delta P$. This unknown constant may be implicitly given by prescribing the flow rate (or the mean velocity at a cross section). In the case of temperature solution, the scheme described above requires modification. This is because the inlet and outlet temperatures will not be the same due to heat transfer from the cylinder. A uniform temperature is applied to the tube surface and at inlet or outlet, the mean temperature rise in the solution domain is subtracted or added depending on whether the boundary condition information is transferred backward or forward.

## NUMERICAL METHODOLOGY

Time marching approach is used and the solution procedure is carried out iteratively within each time step, due to the complex nature of boundary conditions prescribed. At time $t = 0$, to start the iteration process, a uniform velocity profile is assumed at inlet. During each cycle of iteration, symmetric boundary conditions for in-line cylinders and anti-symmetric boundary conditions for staggered cylinders, as described above, are imposed at the inlet, from the predictions at the outlet boundary. In the case of temperature, the scheme described above is modified to account for the fact that due to heat transfer from the cylinder, the inlet and exit temperatures are not same. A uniform temperature $T_H = 1.0$ is applied at the cylinder surfaces. At time $t = 0$, a uniform temperature profile $T_{\text{in}} = 0$ is assumed at the inlet. During each cycle of iteration, temperatures at the outlet are obtained by interpolation from the two upstream nodes and the mean temperature rise across the solution domain is subtracted to obtain the inlet temperature profile.

The Reynolds number is defined as $Re = (\rho u d)/\mu$, where $u$ is the mean velocity at the minimum cross sectional area. The friction factor for one row of tubes can be written as

 

following Zhukauskas and Ulinkas [12]

$$f = \frac{1}{2}\frac{\Delta P}{\rho u^2} \tag{11}$$

The local Nusselt number is obtained from a three-point polynomial fit for the temperature profile ($Nu = \partial T^*/\partial n$) and the average Nusselt number at the cylinder surface is obtained from

$$Nu_{av} = \frac{\int_0^\theta \frac{\partial T^*}{\partial n}\,\mathrm{d}\theta}{\int_0^\theta \mathrm{d}\theta} \tag{12}$$

where $T^*$ is the non-dimensional temperature $[(T - T_b)/(T_w - T_b)]$, $T_w$ is the cylinder wall temperature and $T_b$ is the bulk temperature.

The average inlet and outlet temperatures are given as

$$T_{\text{in}} \text{ or } T_{\text{out}} = \text{average inlet or outlet temperature} = \frac{\int_0^y \rho u T(y)\,\mathrm{d}y}{\int_0^y \rho u\,\mathrm{d}y}$$

## VALIDATION

For validating the numerical predictions, analysis for the fluid flow and heat transfer over a bank of in-line cylinders (Figure 3) is carried out for which there is experimental data. The geometrical parameters in this case are

$$S_T/d = 1.25;\ S_L/d = 1.25 \text{ and } d = 1.0.$$

where $S_T$ is the transverse pitch and $S_L$ is the longitudinal pitch as shown in Figure 1(a).

Studies are carried out for three different cases of Reynolds number, $Re = 50, 100$ and 250. Based on a grid independence study, $143 \times 81$ grid points are used for computation. The predicted results for friction factor and Nusselt number for $Re = 50, 100$ and 250 agree very well with the experimental results of Zhukauskas and Ulinkas [12] and Bergelin *et al.* [3] as shown in Figure 5.

Another validation is carried out for flow over a bank of staggered cylinders (Figure 4). The geometrical parameters in this case are

$$S_T/d = 2.0; \quad S_L/d = 2.0 \text{ and } d = 1.0$$

Results are predicted for three different cases of Reynolds number, $Re = 40, 120$ and 400. The predicted results for Nusselt number and separation angle are shown in Table I .

It can be seen that the results of the present study agree very well with the numerical results of Chen and Wung [13] and Wung and Chen [16].

With the confidence obtained from these validations, the following detailed study is carried out in order to investigate the local physical aspects of fluid flow and heat transfer under different conditions.

## FLOW OVER A BANK OF STAGGERED CYLINDERS

An extensive study is carried out to simulate the steady state flow and convective heat transfer phenomena for flow over a bank of staggered cylinders, arranged in equitriangular pitch as

 

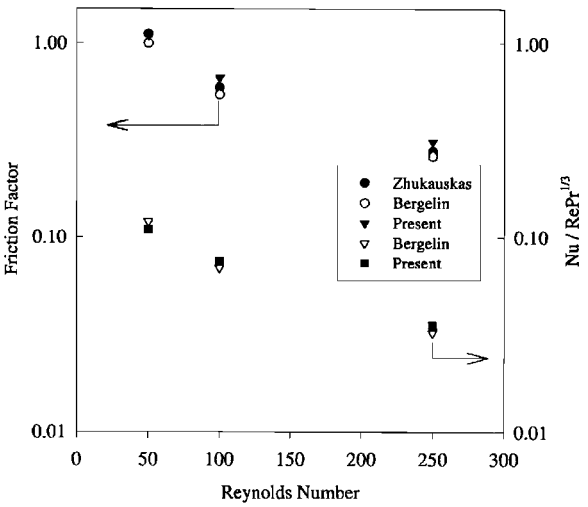


Figure 5. Variation of friction factor and Nusselt number for different Reynolds number for in-line cylinders.

Table I. Predicted results of Nusselt number and separation angle.

| *Re* | Nusselt number | | Separation angle ($\theta_s$), degree | |
|---|---|---|---|---|
| | Present | Chen and Wung [13] | Present | Wung and Chen [16] |
| 40 | 4.053 | 4.102 | 30 | 38 |
| 120 | 6.806 | 6.726 | 49 | 54 |
| 400 | 10.747 | 11.562 | 60 | 66 |

shown in Figure 1(b). It is assumed that the flow is symmetric with respect to the top and bottom boundaries of the computational domain and is periodic anti-symmetric with respect to inlet and outlet portions. In other words, unsteady asymmetric vortex shedding behind the cylinder has not been considered and for this reason the maximum Reynolds number value has been restricted to 1000 for each cylinder spacing.

Computations are made for the pitch-to-diameter ratios ($S_d/d$) of 1.25, 1.5 and 2 and Reynolds number values of 40, 75, 150, 200, 250, 500, 750 and 1000. For each study, an initial mesh of $42 \times 21$ grid points is used for computation and the number of grid points is increased progressively till grid independent results are obtained. Based on the grid independence study, the following grids in Table II are chosen for computations.

In the above grid specifications, the first dimension represents the number of nodes in the flow direction and the second dimension denotes the number of nodes in the transverse direction. The converged solution for a lower Reynolds number is used as the initial guess for the next higher Reynolds number to reduce the computational time.

 

Table II. Grids chosen for computation.

| $S_d/d$ | Grid Points |
|---|---|
| 1.25 | $82 \times 41$ |
| 1.50 | $82 \times 61$ |
| 2.00 | $82 \times 81$ |

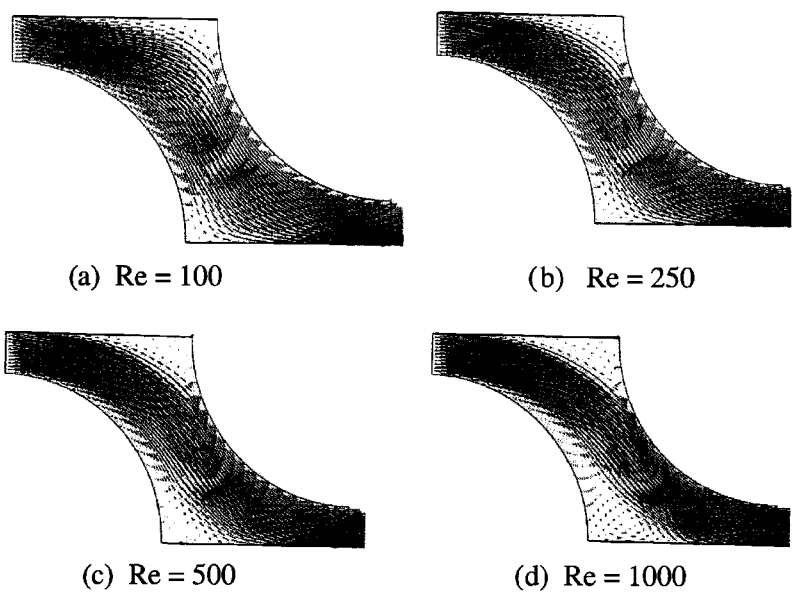


Figure 6. Velocity vectors in staggered cylinders for pitch-ratio = 1.25.

*Flow behaviour*

The variations in the flow structure at different Reynolds number and pitch-to-diameter ratios ($S_d/d$) are shown in Figures 6–8, with the help of velocity vectors.

For a pitch-to-diameter ratio of 1.25, the flow almost completely fills the non-uniform gap between the cylinders, when Reynolds number is equal to 100 (Figure 6(a)). Small stagnation zones are observed in the front part of the second cylinder and the rear part of the first cylinder, which are not accessed by the flow. At higher Reynolds number (for the same pitch-to-diameter ratio), both the stagnation zones increase (Figure 6(b)–(d)). The stagnation zone in the rear region of the first cylinder increases in size at a faster rate and recirculatory flow is observed in this region for $Re = 1000$. A relatively weaker recirculatory zone appears near the front part of the second cylinder also. Due to the growth of stagnation/recirculation regions, the width of flow passage is reduced and a high-speed stream of narrow width is seen at higher Reynolds number, which by-passes the front or rear regions of the cylinders. Similar features are observed for the higher pitch-to-diameter ratio of 1.5 also, as shown in Figure 7(a)–(d). The main differences, however, are that recirculatory flow occurs at a lower

 

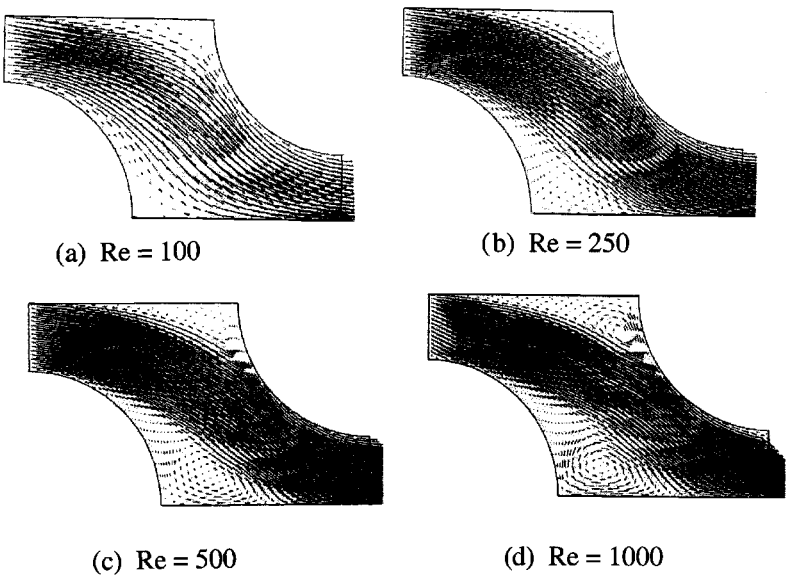


Figure 7. Velocity vectors in staggered cylinders for pitch-ratio = 1.5.

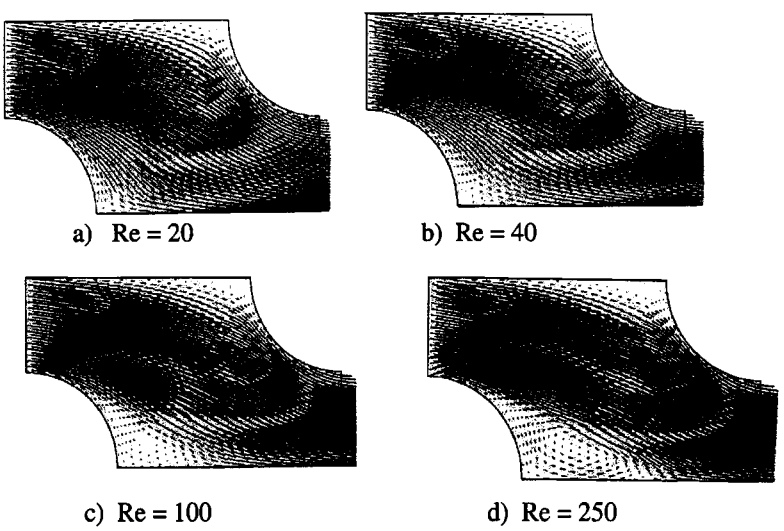


Figure 8. Velocity vectors in staggered cylinders for pitch-ratio = 2.0.

Reynolds number itself ($Re = 250$) and moreover, the sizes of the recirculatory zones are larger at the same Reynolds number, as compared to the case of $S_d/d = 1.25$. These trends are continued for the $S_d/d$ ratio of 2.0 also, as shown in Figure 8(a)–(d). Recirculatory flow

 

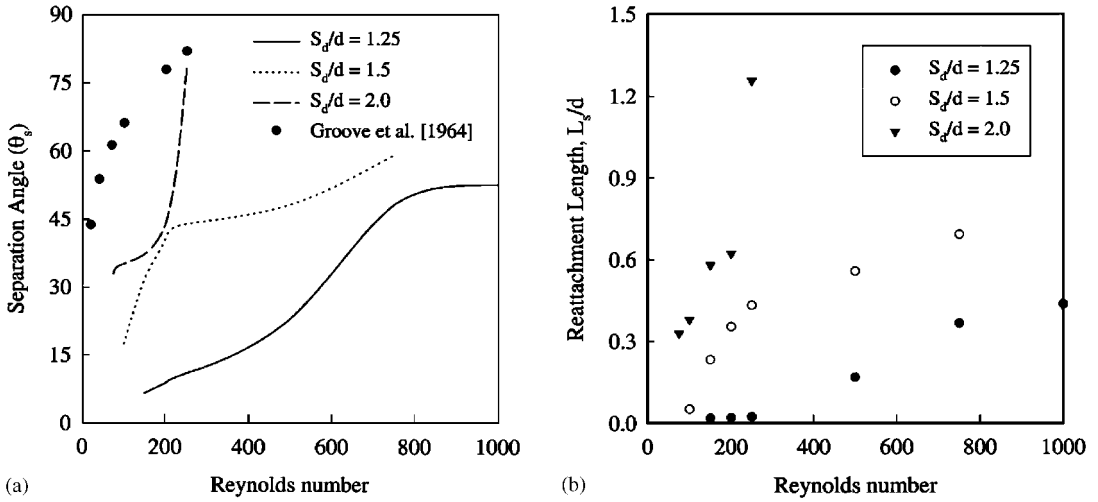


Figure 9. Variation of separation angle and reattachment length for staggered cylinders at different pitch-ratios. (a) Variation of separation angle for different Reynolds number; (b) variation of reattachment length for different Reynolds number.

in the rear stagnation region of the first cylinder begins at $Re = 100$ itself and when $Re$ is increased to 250, the recirculatory flow almost covers up to $\theta = 90°$ for the first cylinder. For this reason, simulation is not extended beyond $Re = 250$, since the recirculatory flow will interfere with the prescribed flow conditions at the inlet sections.

The variation of separation angle, $\theta_s$ and the reattachment length, $L_s$ in the rear portion of the first cylinder are plotted against $Re$, at various $S_d/d$ values (Figure 9(a) and (b)). It is evident that flow separation angle and reattachment length increase with both Reynolds number and pitch-to-diameter ratio. While the increase is gradual in the cases of $S_d/d = 1.25$ and 1.5, it is very steep in the case of $S_d/d = 2.0$. For the sake of comparison, the trend for a free cylinder is also included in Figure 9(a). It is evident that the values of flow separation angle and reattachment length approach those for a free cylinder, when the gap between the cylinders increases.

### *Temperature distribution*

The typical shapes of isotherms for different Reynolds numbers and spacing between cylinders are shown in Figure 10(a)–(f). For low Reynolds number and small gap (Figure 10(a)), the heating effect penetrates into the entire fluid between the cylinders, as seen from the higher isotherm values. For a higher Reynolds number and small gap (Figure 10(b)), heating is primarily confined to the boundary layers over both the cylinders. The thickness of the boundary layers is observed to grow in the direction of flow. In the rear portion of the first cylinder, however, the effects of recirculatory flow are observed very close to $\theta = 180°$. For $S_d/d = 1.5$ and $Re = 250$ (Figure 10(c)), the heat affected zone is relatively smaller than that for $S_d/d = 1.25$ (Figure 10(a)). However, the influence of recirculation in the rear part is seen at $Re = 250$ itself for the case of $S_d/d = 1.5$. At a Reynolds number of 500 (Figure 10(d)), it is seen that the recirculatory region has relatively low temperatures due to back mixing of

 

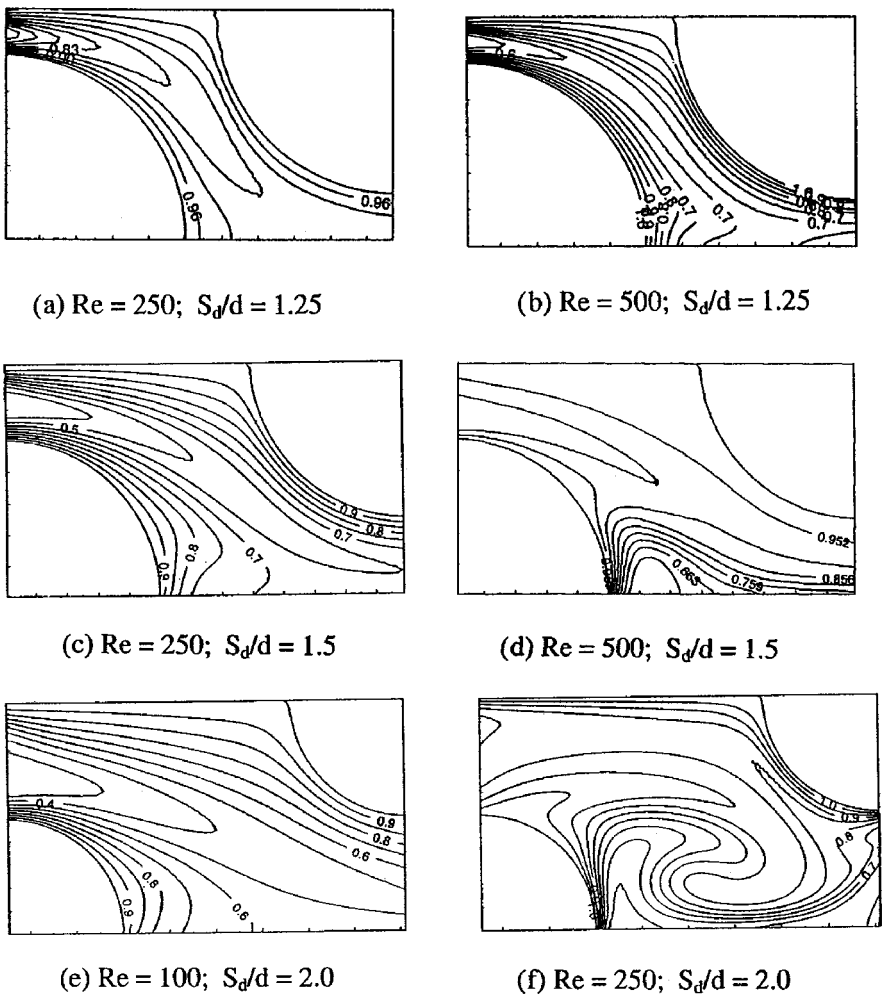


Figure 10. Isotherms for different pitch-ratios and Reynolds number in staggered cylinders.

the cold free stream fluid with the heated boundary layer fluid. These features are accentuated further in Figure 10(e) and (f), which correspond to $Re = 100$ and $Re = 250$ respectively, for $S_d/d = 2.0$. In particular, the severe distortions in the shapes of isotherms due to back mixing caused by recirculatory flow are evident in Figure 10(f).

*Nusselt number variation*

The Nusselt number variations along the front and rear cylinders are plotted in the angular ranges of $\theta = 0°$ to $90°$ and $\theta = 180°$ to $270°$, respectively in Figure 11(a)–(c). In both the cases, $\theta$ is measured from rear of the cylinder ($\theta = 0°$) anti-clockwise from the flow direction. The following trends are evident from the figures. For the first cylinder (A) local

 

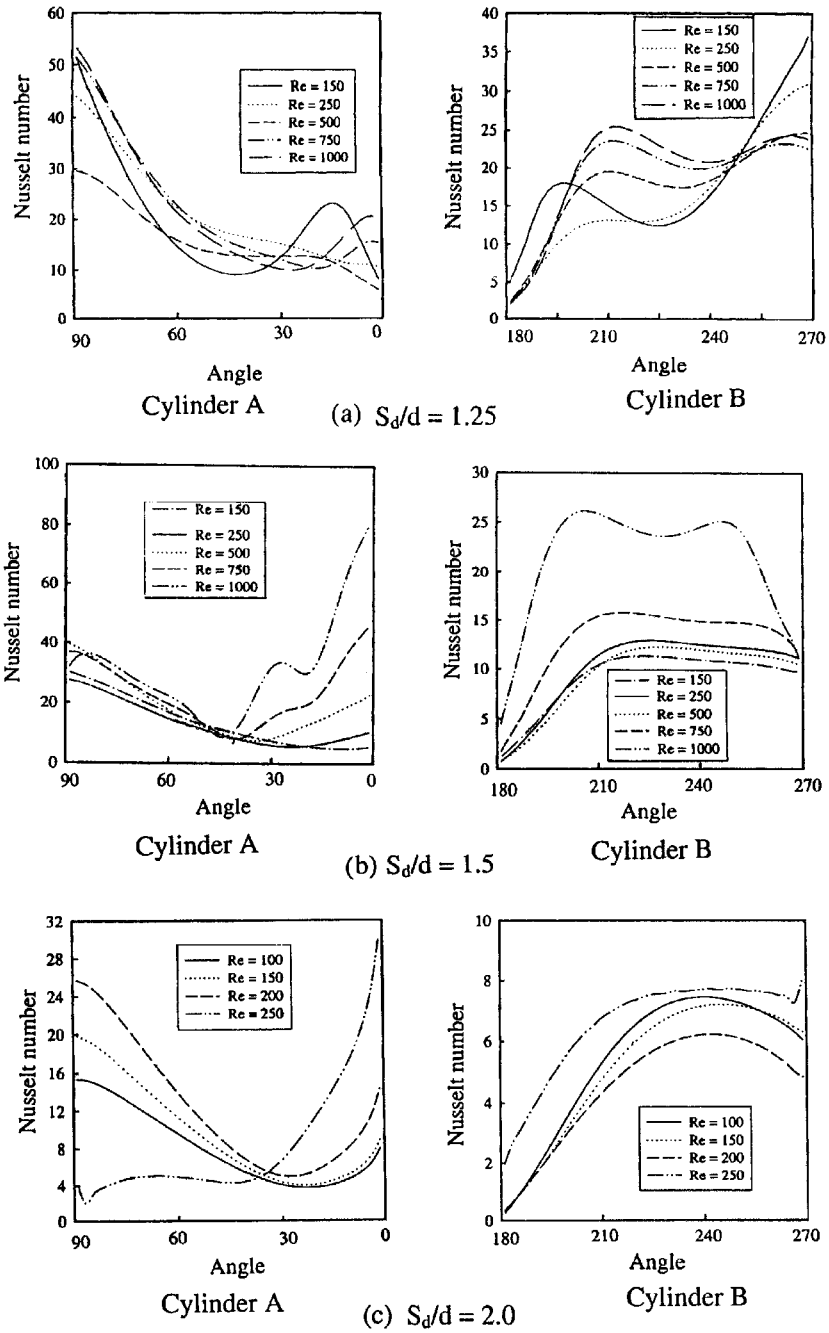


Figure 11. Variation of local Nusselt number along the cylinder surface for different pitch-ratios in staggered cylinders.

 

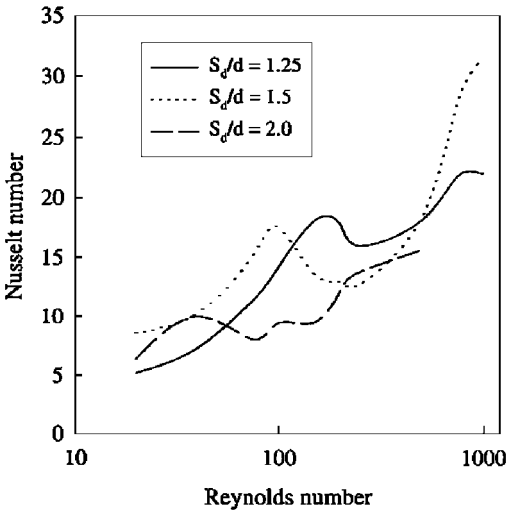


Figure 12. Variation of average Nusselt number for different pitch-ratios and Reynolds number in staggered cylinders.

Nu is maximum at the inlet section ($\theta = 90°$) and it decreases in the flow direction (decreasing $\theta$) up to a maximum value and then increases again in the rear portion of the cylinder (close to $\theta = 0°$). The initial decrease of Nu in the flow direction can be explained as due to thermal boundary layer growth and the separation of flow from the cylinder surface before reaching the rear stagnation point. Beyond the separation point, due to recirculatory flow, Nu again increases in the flow direction up to rear stagnation point. However, in addition to more general trends, the local Nu also exhibits some undulations due to variation in the cross-sectional area in the gap between the cylinders.

As regards the second cylinder (B), Nu has a minimum value at the front stagnation point ($\theta = 180°$) due to the stagnation fluid zone prevailing there. With increase in angle, the main flow attaches to the cylinder and a local maximum is then observed in the Nu value corresponding to the flow attachment point. With further increase in $\theta$, Nu decreases due to growth of the thermal boundary layer. But eventually assumed $\theta = 270°$ (outflow boundary), the Nusselt number again increases due to the convergence of stream lines caused by the reduction in flow area. Thus, the local Nusselt number variation on each cylinder shows a complex pattern at different *Re* and pitch-to-diameter ratio values, due to occurrence of stagnation or recirculation zones, thermal boundary layer growth and changes in the flow cross-sectional area in the direction of flow.

The average Nusselt number (considering heat transfer from both cylinders) variation with Reynolds number is shown in Figure 12, for different pitch-to-diameter ratios. For each spacing, the average Nu is seen to increase with *Re* initially, attain a peak value, decrease slightly with further increase in *Re* and finally increase once again with *Re* until it leaves off at a second maximum value. These trends can be attributed to the changes in flow structure which take place in the gap between the cylinders, as follows. Average Nu increases with *Re* initially, because of the establishment of thin boundary layers. As seen from the flow structures

 

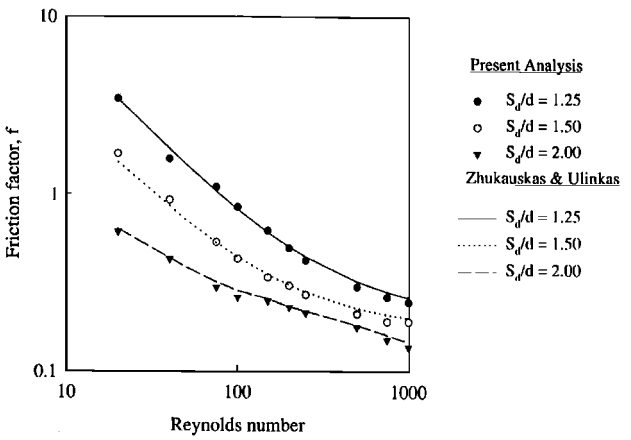


Figure 13. Variation of friction factor for flow over staggered cylinders for different pitch-ratios.

of Figures 6–8, for higher *Re*, stagnant fluid zones develop in the rear and front portions of the first and second cylinders respectively. These stagnant zones cause poor heat transfer between the cylinders and the fluid. Therefore, average Nu decreases with Reynolds number. However, with further increase in *Re*, flow recirculation causes back mixing and hence local heat transfer rate increases due to larger $\Delta T$ in the recirculation zone. This reflects as an increase in the corresponding average Nu value. Eventually, at still higher *Re*, the average Nusselt number magnitude levels off because the recirculatory eddy attains its maximum size (upto a separation angle of $\theta_s \approx 90°$), in the confined region between the two cylinders. As regards the effects of $S_d/d$ ratio, it is evident that the maxima and minima of average Nu shift towards lower Reynolds number values for larger spacing; this is easily explained from the fact that the stagnant zone and recirculatory flow occur at lower Reynolds number when the gap between the cylinder is increased.

*Pressure drop across bank of cylinders*

Figure 13 gives the computed friction factor values with the empirical correlations suggested by Zhuskauskas and Ulinkas [12]. The comparison shows that the predicted results agree very well with the data of Zhuskauskas and Ulinkas [12] at all the pitch-to-diameter ratios. For the laminar flow range considered in the present study, the friction factor varies approximately in inverse proportion to the Reynolds number, as expected.

## SUMMARY

Numerical simulation is carried out for laminar fluid flow and heat transfer over a bank of in-line and staggered cylinders. The relative spacing between the cylinders is found to have a strong effect on the flow pattern and heat transport properties. At low spacing, the neighbouring cylinder suppresses eddy formation behind the front cylinder and as the spacing increases; recirculatory vortex is generated at a relatively lower Reynolds number. For low Reynolds

 

number, thermal diffusion is the major mode of heat transfer whereas at higher Reynolds number convective heat transfer is predominant. The velocity, pressure and temperature profiles obtained are physically consistent and the friction factor agrees excellently with the available experimental data.

ACKNOWLEDGEMENTS

The authors wish to thank Mr Joseph Winston of IGCAR, Kalpakkam for rendering all help and providing the software for the vector plots.

## NOTATION

*English symbols*

| | |
|---|---|
| $A$ | Area |
| $a$ | Coefficients of discretized equations |
| $b$ | Component of source term |
| $C_P$ | Specific heat |
| $d$ | Coefficient of diffusive flux; diameter of the cylinder |
| $F$ | Mass flux |
| $g$ | Acceleration due to gravity |
| $h$ | Convective heat transfer coefficient |
| Nu | Local Nusselt number (h d/$\lambda$) |
| $P$ | Dynamic pressure ( = total pressure – hydrostatic pressure) |
| $\dot{Q}$ | Volumetric heat generation |
| $S$ | source term; pitch for the bank of cylinders |
| $T$ | Temperature |
| $T_{in}$ | Inlet temperature (average) |
| $T_{out}$ | Outlet temperature (average) |
| $t$ | Time |
| $u, v$ | Cartesian velocity components |
| $u_\infty$ | Average approach velocity for flow over cylinders |
| $V$ | Volume of a cell |
| $x, y$ | Co-ordinate directions |

*Greek symbols*

| | |
|---|---|
| $\alpha$ | Thermal diffusivity ($\lambda/\rho C_P$); under-relaxation factor for iterative solution |
| $\Gamma$ | Coefficient for diffusive flux |
| $\lambda$ | Thermal conductivity |
| $\mu$ | Dynamic viscosity |
| $\theta$ | Angular co-ordinate on the cylinder surface |
| $\rho$ | Density |
| $\tau$ | Stress tensor component |

 

*Subscripts*

| | |
|---|---|
| $e, w, n, s$ | Values associated with control volume faces |
| $E, W, N, S$ | Values associated with centres of neighbouring control volumes |
| $ne, nw, se, sw$ | Values associated with control volume vertices |
| $k$ | For control volume face k |
| $i, j$ | Co-ordinate direction indices |
| $nb$ | Neighbouring node |
| $P$ | Pressure; values associated with centre of the control volume |
| $u$ | For velocity variable |
| $t$ | For temperature |

*Superscripts*

| | |
|---|---|
| $'$ | Correction increment |
| $*$ | Uncorrected values (predictor step) |
| 1, 2 | Orthogonal and non-orthogonal term index |
| $o$ | Initial guess value |

## REFERENCES


1. Pierson OL. Experimental investigation of the influence of tube arrangement on convective heat transfer and flow resistance in cross flow of gases over tube banks. *ASME* 1937; **59**:563–572.
2. Bergelin OP, Davis ES, Hull HL. A study of three tube arrangements in unbaffled tubular heat exchangers. *Transactions of the ASME* 1949; **71**:369–374.
3. Bergelin OP, Brown GA, Hull HL, Sullivan FW. Heat transfer and fluid friction during viscous flow across banks of tubes—III. A study of tube spacing and tube size. *Transactions of the ASME* 1950; **72**:881–888.
4. Zhukauskas A. Heat Transfer from tubes in cross flow. *Advances in Heat Transfer* 1989; **8**:72–160.
5. Thom A, Apelt CJ. *Field Computations in Engineering and Physics*. Van Nostrand; London, 1961.
6. Le Feuvre RF. Laminar and Turbulent Forced Convection Processes through In-line Tube Banks. Imperial College London, Mech. Engng. Dept. 1973; *HTS/74/5*.
7. Faghri M, Rao N. Numerical computation of fluid flow and heat transfer in finned and unfinned tube banks. *International Journal of Heat Mass Transfer* 1987; **30**:363–372.
8. Launder BE, Massey TH. The numerical prediction of viscous flow and heat transfer in tube banks. *ASME Journal of Heat Transfer* 1978; **100**:565–571.
9. Roychowdhury DG, Das Sarit K, Sundararajan T. An efficient solution method for incompressible N–S equations using non-orthogonal collocated grid. *International Journal for Numerical Methods in Engineering* 1999; **45**: 741–763.
10. Segal G, Vuik K, Kessels K. On the implementation of symmetric and anti-symmetric periodic boundary conditions for incompressible flow. *International Journal for Numerical Methods in Fluids* 1994; **18**: 1153–1165.
11. Bai L, Mitra NK, Fiebig M, Kost A. A multigrid method for predicting periodically fully developed flow. *International Journal for Numerical Methods in Fluids* 1994; **18**:843–852.
12. Zhukauskas A, Ulinkas R. Banks of plain and finned tubes. *Heat Exchanger Design Handbook*. Hemisphere Publishing Corporation: Washington, 1983; **2**:Section 2.2.4.
13. Chen CJ, Wung TS. Finite analytic solution of convective heat transfer for tube arrays in cross flow, Part 2: Heat transfer analysis. *ASME Journal of Heat Transfer* 1989; **111**:641–648.
14. Patankar SV, Spalding DB. A calculation procedure for heat, mass and momentum transfer in three-dimensional parabolic flows. *International Journal of Heat Mass Transfer* 1972; **15**:1787–1806.
15. Kobayashi MH, Pereira CF. Calculation of incompressible laminar flows on a non staggered, non-orthogonal grid. *Numerical Heat Transfer* (Part B) 1991; **19**:243–262.
16. Wung TS, Chen CJ. Finite analytic solution of convective heat transfer for tube arrays in cross flow, Part 1: Flow field analysis. *ASME Journal of Heat Transfer* 1989; **111**:633–640.
17. Groove AS, Shair FH, Peterson EE, Acrivos A. An experimental investigation of steady flow past a circular cylinder. *Journal of Fluid Mechanics* 1964; **19**:1223–1239.


 